

# Nanoscale movements of cellulose microfibrils in primary cell walls

Tian Zhang<sup>1</sup>, Dimitrios Vavylonis<sup>2</sup>, Daniel M. Durachko<sup>1</sup> and Daniel J. Cosgrove<sup>1\*</sup>

The growing plant cell wall is commonly considered to be a fibre-reinforced structure whose strength, extensibility and anisotropy depend on the orientation of crystalline cellulose microfibrils, their bonding to the polysaccharide matrix and matrix viscoelasticity<sup>1–4</sup>. Structural reinforcement of the wall by stiff cellulose microfibrils is central to contemporary models of plant growth, mechanics and meristem dynamics<sup>4–12</sup>. Although passive microfibril reorientation during wall extension has been inferred from theory and from bulk measurements<sup>13–15</sup>, nanometre-scale movements of individual microfibrils have not been directly observed. Here we combined nanometre-scale imaging of wet cell walls by atomic force microscopy (AFM) with a stretching device and endoglucanase treatment that induces wall stress relaxation and creep, mimicking wall behaviours during cell growth. Microfibril movements during forced mechanical extensions differ from those during creep of the enzymatically loosened wall. In addition to passive angular reorientation, we observed a diverse repertoire of microfibril movements that reveal the spatial scale of molecular connections between microfibrils. Our results show that wall loosening alters microfibril connectivity, enabling microfibril dynamics not seen during mechanical stretch. These insights into microfibril movements and connectivities need to be incorporated into refined models of plant cell wall structure, growth and morphogenesis.

To visualize microfibril movements, we prepared cell-free strips of the outer epidermal wall of onion (Fig. 1a), because this material is suitable for both tensile tests<sup>14,16,17</sup> and high-resolution AFM imaging of individual microfibrils at the inner (newly deposited) cell wall surface<sup>18</sup>. AFM also let us assess the wall surface by nano-mechanical methods. To modulate wall stress and strain, wall strips were clamped in a custom-made extensometer (Supplementary Fig. 1) mounted on the AFM stage. Before mounting, the wall was washed gently to remove adherent membranes and cytoplasm and heated for 10 s to inactivate endogenous enzymes, but otherwise was in a near-native state. The wall was submerged under a buffer throughout the experiments.

A well-defined series of axial extensions (Fig. 1b,c) resulted in consecutive plastic deformation, elastic deformation, time-dependent stress relaxation and irreversible extension ('creep') of the wall. This protocol was based on the well-established biomechanical behaviour of primary cell walls<sup>19</sup> (see Methods): plastic deformation occurs when the wall is stretched beyond its yield point and is gauged as the residual extension after the force is re-zeroed (Fig. 1b,c). A second extension that does not exceed the first stretch point is reversible, thus elastic (Supplementary Fig. 2). Stress relaxation was induced by holding the wall length constant and adding Cel12A, a  $\beta$ 1,4-endoglucanase that loosens load-bearing junctions between microfibrils<sup>20</sup>. After a period of stress relaxation, the wall was freed to extend, converting relaxation into

wall creep. Cel12A treatment mimics auxin-induced wall loosening<sup>21–23</sup>, resulting in wall stress relaxation and creep that are essential for cell growth<sup>3,24</sup>.

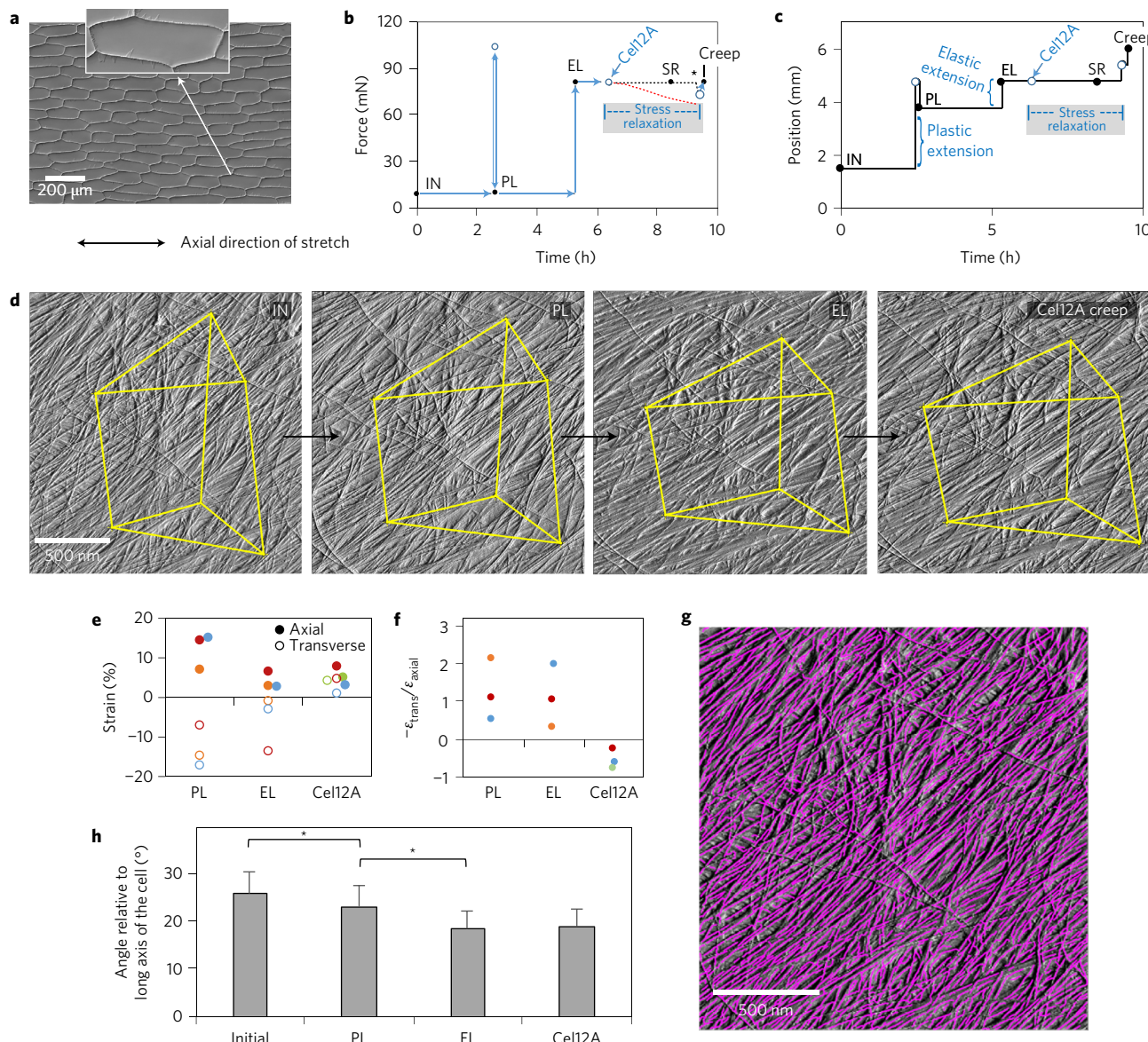
AFM images of the same surface ( $2 \times 2 \mu\text{m}^2$ ) were collected after these sequential steps to follow displacements of the same collection of microfibrils (Fig. 1d). This cell wall is a polylamellate structure with cellulose microfibrils (3 nm wide) forming a trellis-like network of bundled microfibrils that are oriented within each lamella in a common direction that shifts by 30–90° between adjacent lamellae<sup>18</sup>. By close inspection of the images we identified points where two microfibrils intersected without evidence of local microfibril sliding during wall extension. These stable intersections were treated as fiducial marks to calculate micrometre-scale axial and transverse extensions (strains). To aid visual comprehension of the overall pattern of surface distortions, some of these points are joined by yellow lines in Fig. 1d.

Under plastic and elastic strains, the wall stretched axially and compressed transversely (Fig. 1e), resulting in a mean strain ratio ( $-\varepsilon_{\text{trans}}/\varepsilon_{\text{axial}}$ ) of  $\sim 1$  (Fig. 1f). For elastic strains this is called Poisson's ratio, which ranges from 0 to 0.5 in many polymeric materials. The high value for plant cell walls has been attributed to the arrangement of stiff cellulose microfibrils in the plane of the wall and their relative freedom to reorient<sup>16</sup>. Transverse compression on axial extension indicates mechanical coupling between microfibrils, potentially at limited junctions dubbed 'biomechanical hotspots'<sup>20</sup>.

To compare these forced mechanical strains with wall yielding catalysed by wall loosening<sup>21</sup>, we treated elastically stretched walls with Cel12A<sup>20</sup> to stimulate wall stress relaxation and creep, biophysical processes essential for cell growth<sup>3,23,24</sup>. During stress relaxation (shaded box in Fig. 1b), microfibril movement was negligible at the micrometre-scale (Supplementary Video 1). To end the relaxation phase, the locked stage was released and the holding force was manually restored to the elastic set point (Fig. 1b,c). The enzymatically loosened wall extended both axially and transversely (Fig. 1d,e), resulting in a ratio ( $-\varepsilon_{\text{trans}}/\varepsilon_{\text{axial}}$ ) of approximately  $-0.5$ . Negative Poisson's ratios occur during elastic strain of so-called auxetic materials as a result of honeycomb-like or hinged microstructures<sup>25</sup>, but in the case of Cel12A action the negative value is likely to result from mechanical decoupling of microfibrils, freeing them to separate in the direction of applied force while simultaneously releasing the transverse compression that arose during prior elastic extension. Hence, enzymatic loosening alters microfibril connectivity, enabling wall creep via patterns of microfibril movement different from those occurring during forced mechanical extension.

This conclusion is confirmed at the nanometre scale by visual inspection of the AFM images which show appreciable angular reorientations of microfibrils after plastic and elastic strains, but not after creep (seen most strikingly by comparing

<sup>1</sup>Department of Biology and Center for Lignocellulose Structure and Formation, Penn State University, University Park, 208 Mueller Laboratory, Pennsylvania 16802, USA. <sup>2</sup>Department of Physics, Lehigh University, Bethlehem, Pennsylvania 18015, USA. \*e-mail: dcogrove@psu.edu



Supplementary Videos 2–4). Previous work likewise did not detect altered microfibril angle after creep of cucumber hypocotyl cell walls<sup>26</sup>. To quantify microfibril orientations by automated analysis we used image analysis software to identify microfibril segments ('snakes', Fig. 1g) and their orientations. Microfibrils progressively realigned in the stretch direction after plastic and elastic extensions,

whereas their orientation remained statistically unchanged after Cel12A-induced creep (Fig. 1h), despite greater axial strain than transverse strain. These results show that passive microfibril reorientation—the foundation of the multinet growth hypothesis<sup>13</sup>—indeed contributes to axial extension and transverse compression when the cell wall is passively stretched by external force, but not

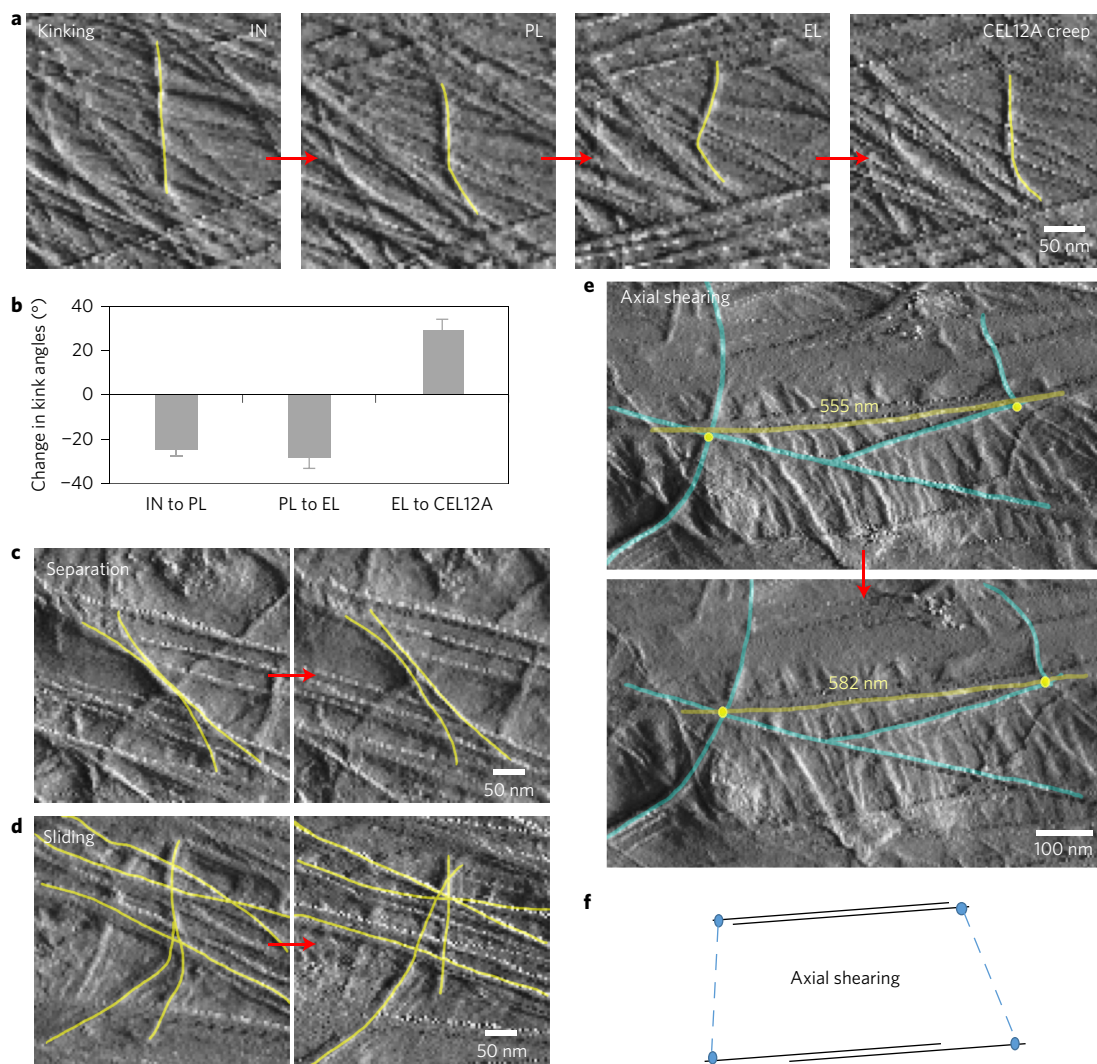


**Figure 2 | Diversity of individual microfibril movements during cell wall extension.** **a**, AFM Peakforce error images showing the dynamics of microfibril kinking during four points in the extension series. **b**, Average changes in kink angles between consecutive points in the extension series. Error bars are the s.e.m.  $28 \leq n \leq 41$  from three replicate experiments. All means are significantly different from zero. **c**, An example of lateral separation of two microfibrils during elastic extension. Note that axially oriented microfibrils draw closer together, correlating with transverse compression. **d**, An example of independent motions (sliding and separation) of microfibrils in adjacent lamellae during Cel12A creep. **e**, An example of axial shearing (side-by-side gliding) of microfibrils during elastic extension. **f**, A diagram to clarify axial shearing of microfibrils. In **a** and **c–e**, the yellow lines were added to highlight microfibrils of interest. These four classes of motion were observed during plastic, elastic and Cel12A-induced movements.

during enzyme-mediated creep. The results challenge the idea—often asserted in discussions of cell growth and implicitly inferred by contemporary finite-element models of plant morphogenesis<sup>4,7,9–11,27</sup>—that elastic strain is the initial step for cell wall growth. Here we see evidence that wall elasticity and creep employ distinctive microfibril motions.

Closer inspection of the AFM images revealed additional clues about how microfibrils are interconnected and anchored in the cell wall: (1) most microfibril segments in this wall are aggregated into bundles of two to five microfibrils<sup>18</sup>; during plastic and elastic strains the bundles reoriented as cohesive units, reshaping the pliant matrix between the bundles. Lateral bonding between microfibrils within a bundle was evidently stable enough to withstand the shear forces generated during these extensions and when the AFM tip repeatedly scanned the wall surface. (2) The two or three lamellae visible in the AFM images deformed coherently, without micrometre-scale slippage between lamella (although limited slippage was seen at the nm-scale, described below). We take this to mean that adjacent lamellae are firmly connected to

each other and are not free to deform individually as dictated by their distinctive microfibril orientations. (3) Microfibrils transverse to the applied axial force became curved or kinked during plastic and elastic extensions (Figs 1d and 2a,b; Supplementary Videos 2,3), a result of transverse compression of the wall and the inability of stiff microfibrils to accommodate appreciable compression along the microfibril axis. After Cel12A-induced creep, the kinked microfibrils became straighter, consistent with the action of this enzyme to loosen load-bearing junctions between microfibrils<sup>20</sup>, reversing the transverse compression imposed during the preceding axial stretch. (4) Lateral shifts of kinked or curved microfibrils indicate that microfibrils are not firmly anchored throughout their length but rather at uneven intervals, roughly estimated from the kinked segments to be  $\sim 100\text{--}200$  nm. Between anchor points the microfibrils appear free to move. This distance may correspond to the spacing of load-bearing junctions in the microfibril network of this cell wall and is similar to the estimated density of binding sites in cell walls for expansins<sup>28</sup>, the endogenous wall-loosening proteins in plants<sup>21</sup>. Additional microfibril motions seen in this

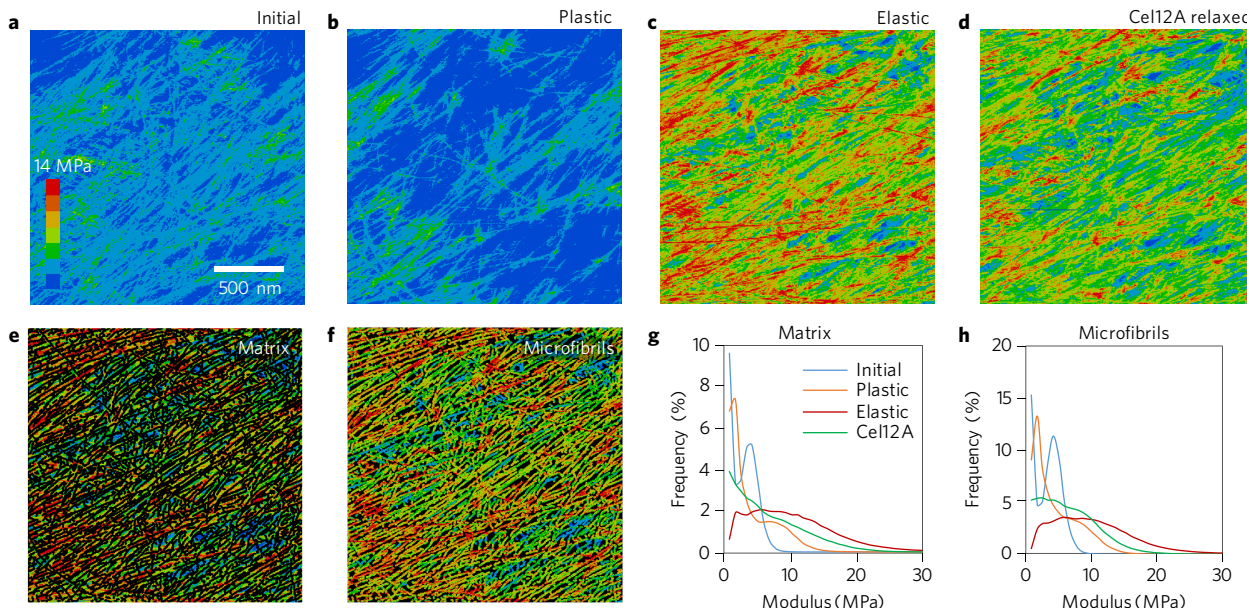


**Figure 3 | Modulus maps of cell wall surface after different modes of extension.** **a-d**, Heat maps of indentation modulus of the cell wall surface at four points in the extension series, collected in Peakforce tapping mode simultaneously with the images in Fig. 1d. The colour scale is at the left (step size = 2 MPa). Note that the modulus of axially aligned microfibrils is particularly reduced after Cel12A relaxation, indicating non-homogeneous stress relaxation at the nanoscale. The modulus values increase when the holding force is restored (Supplementary Fig. 5). **e**, A modulus map of the matrix component of the image in **c**, obtained by blacking out microfibrils identified with SOAX. **f**, A modulus map of the microfibril component of the image in **c**, identified by SOAX software. **g**, Histograms of the modulus distribution for the matrix for images **a-d**. **h**, Histograms of the modulus distribution for the microfibrils during four extension points shown in **a-d**. Note the y axes in **g** and **h** differ by a factor of two and that values of 0–1 MPa are not plotted on the graph because of scaling issues (see Supplementary Fig. 4 for an example of the complete distribution). This experiment was replicated three times with similar results. IN, initial; PL, plastic; EL, elastic.

study include lateral separation of microfibrils (Fig. 2c), sliding of microfibrils across one another (Fig. 2d) and axial shearing (side-by-side gliding) of aligned microfibrils (Fig. 2e,f). These results expand the repertoire of microfibril motions beyond the oft-discussed notion of passive angular reorientation.

This series of wall extensions was also analysed by nanomechanical mapping, which assesses local resistance to surface indentation by the AFM tip, quantified as a modulus<sup>29</sup>. The presence of fibrillar features in the modulus maps (Fig. 3a–d) indicates microfibrils resist indentation more than does the matrix. This is due partly to microfibril stiffness and partly to microfibril support by the underlying matrix and by contacts with other microfibrils. After plastic deformation the modulus map changes, becoming more heterogeneous, accentuating microfibrils and deemphasizing the matrix (Fig. 3b). Plastic deformation evidently rearranges local internal stresses and interactions between matrix polymers and microfibrils. Matrix softening is evidenced by higher correlation between modulus and height after plastic deformation (Supplementary Fig. 3).

When the wall was elastically extended at a constant holding force, the indentation modulus increased markedly across the whole surface (Fig. 3c), demonstrating that surface lamellae contribute to wall mechanics in these experiments. We liken this mechanical response to the lateral stiffening of a guitar string or drumhead on tensioning. We used image analysis software to segregate microfibrils and matrix into separate modulus maps (Fig. 3e,f) and to derive separate histograms of modulus distributions (Fig. 3g,h). The histograms confirm the visual impressions that the modulus values increase when the wall is tensioned and that microfibrils have a higher indentation modulus than the matrix. This latter point is evidenced in Fig. 3g,h by the roughly two times higher proportion of microfibril pixels with a modulus >1 MPa than with matrix (see also Supplementary Fig. 4). Note that the indentation modulus depends on wall structure and differs from the tensile

modulus of cellulose<sup>30</sup>, which is ~100 GPa. Both microfibrils and the matrix stiffen when the wall is tensioned, suggesting that both components bear in-plane tensile stress. Another possibility is that the matrix alone bears tensile stress and the increased microfibril modulus results from firmer support of the matrix. However, infrared spectroscopy of stretched onion walls indicates that cellulose bears some tensile stress<sup>17</sup>. Since the matrix in this wall is predominately pectin, our AFM results support the idea that pectic polysaccharides contribute to cell wall mechanics<sup>7,8</sup>. Finally, when the wall strip was treated with Cel12A but temporarily held at constant length to permit wall stress relaxation, the indentation modulus decreased in a heterogeneous pattern (Fig. 3d), indicating an uneven nanoscale pattern of relaxation. When the elastic force was restored, modulus values increased in a heterogeneous pattern (Supplementary Fig. 5). These patterns provide further evidence of the 100–200 nm scale of microfibril connectivity.

Our results revealed that microfibril movements in the primary cell wall are strikingly different for extensions motivated by applied forces versus selective wall loosening. How microfibril motions observed here compare with those *in vivo* is uncertain because similar nanoscale studies are not feasible in living cells with current methods. These experiments required removal of the living cell, replacement of turgor-generated wall stresses with uniaxial forces, and replacement of endogenous wall-loosening catalysts with an endoglucanase that mimics loosening caused by auxin<sup>20,22,23</sup>. Living cells may influence microfibril movements and connectivity by additional means. One revealing artefact in these experiments was the microfibril kinking that resulted from uniaxial extension and concomitant transverse compression. We used this kinking artefact as a means to assess microfibril anchoring, rather than to infer movements *in vivo*. Nonetheless, microfibril kinking potentially occurs *in vivo* under some circumstances, for example when gravitropic bending causes wall contractions. The principal

lesson learned here, that mechanically motivated patterns differ from those mediated by wall loosening, is very likely to apply *in vivo* as well. Because plant cells may loosen and stiffen their cell walls in multiple ways, additional insights may be gleaned from further work to characterize microfibril motions at the nanoscale.

This approach could be extended to explore the action of wall-loosening catalysts with other mechanisms of action<sup>21</sup> and to investigate the nanoscale underpinnings of microfibril connectivity for more insightful models that connect wall mechanics to cell growth, morphogenesis and wall integrity sensing. These ideas may also be applicable to the mechanics of other fibre-reinforced biomaterials, such as collagen-based tissues, where, like the plant cell wall, both mechanical and enzymatic factors modulate biomechanical properties.

## Methods

**Preparation of cell walls and mounting on the AFM extensometer.** An epidermal strip, 30 mm long  $\times$  5 mm wide, was excised from the abaxial side of the fifth scale of fresh white onion (*Allium cepa*, cv. Cometa) purchased from a local grocery. As described previously<sup>18</sup>, the outer epidermal walls detached from the rest of the epidermal cells as a large sheet (Fig. 1a), uncovering the wall surface adjacent to the plasma membrane. From photographs of the epidermal surface before and after peeling, we found no evidence that peeling distorted cell shape, other than a small axial shrinkage (~2.5%), presumably because of turgor loss. We used the abaxial epidermis because, unlike the adaxial epidermis, its outer wall readily detaches from the rest of the cells.

The epidermal strip was cut so as to leave a thin trapezoidal prism of parenchyma cells remaining at the two ends, with the cuticle side being the widest base. This helped to orient the wall strip and to keep it from rolling. The long axis of the peel was parallel to the long axis of the epidermal cells and was the stretch direction. The strip was washed in 10 ml of 20 mM HEPES buffer, pH 7.0 with 0.1% Tween-20 for 30 min, then dipped in boiling water for 10 s to inactivate endogenous wall enzymes and expansins. The sample was mounted on a glass slide (75  $\times$  25 mm<sup>2</sup>) with the innermost wall surface facing up and wetted with 20 mM sodium acetate buffer, pH 4.5. With the fixed and movable stages of the extensometer (Supplementary Fig. 1) brought into contact (position 0 mm), the epidermal strip was gently transferred onto the stages with tweezers, aligned to extend the long axis, and wrinkles and air bubbles were removed. The two ends (5 mm) were blotted dry and secured with cyanoacrylate glue (no. GPMR6069) onto the two stages and cover slips (cut to 5  $\times$  10 mm<sup>2</sup>), leaving 20 mm between the fixed ends. A cyanoacrylate accelerator was used to cure the glue immediately. The epidermal strip was kept moist throughout the transfer and fixing process and was completely submerged under buffer throughout the extension and imaging process. The extensometer stage with the cell wall strip was mounted under the AFM scanner head and a liquid column was formed between the AFM probe and the sample by addition of acetate buffer. The imaged region was 7 mm from the fixed end. Visual inspection indicated that transverse mechanical constraint by the fixed ends was limited to regions <2 mm from the glued ends.

**AFM imaging and nanomechanical analysis.** AFM images were collected with a Dimension Icon AFM (Bruker) with ScanAsyst in Peakforce Tapping mode and with Quantitative Nanomechanical Property Mapping (QNM). The AFM tip had a radius of ~1.5 nm and a spring constant between 0.2 and 0.7 N m<sup>-1</sup> (see ref. 18 for details).

**Cell wall extensions.** Our protocol for extending the onion wall was distilled from previous studies of plant cell wall biomechanics which showed that large unilateral mechanical extension includes an irreversible (plastic) component and a reversible (elastic) component<sup>31–33</sup> and that wall-loosening by Cel12A<sup>22</sup> mimics the *in-vivo* wall-loosening effects of auxin treatment<sup>34</sup>. Our tests (Supplementary Fig. 2) confirmed that the macroscale mechanical behaviour of these onion epidermal strips is similar to that reported for other growing cell walls.

Initial slack in the wall strip was removed by extending the sample until a holding force of 5 mN was reached. An initial (IN) AFM image (2  $\times$  2  $\mu\text{m}^2$ ) was collected at this point and the specimen was then extended to a holding force of 100 mN, followed by return to a force of 5 mN, with only partial recovery of the initial length (Fig. 1b,c). The initial image area was located and a second AFM image (PL) was collected. The sample was extended a second time until the holding force reached 80 mN and a third AFM image (EL) of the initial area was collected. Parallel experiments showed this second extension to be reversible and thus elastic (Supplementary Fig. 2). Thereafter the moveable stage (connected to the force sensor) was locked to hold the sample at constant length and 30  $\mu\text{g ml}^{-1}$  Cel12A in 20 mM sodium acetate buffer (pH 4.5) was added to the cell wall sample to induce stress relaxation. Endoglucanase Cel12A, which can hydrolyse both xyloglucan and cellulose and thereby loosen key cellulose–cellulose junctions<sup>20,21</sup>, was expressed in *Escherichia coli* Rosetta-gami (DE3; Novagen), and purified as described<sup>20</sup>. After 2.5 h of Cel12A treatment at constant wall length, a fourth AFM image (Cel12A relaxed)

was collected. Thereafter the moveable stage was released, enabling the force sensor to register the reduced holding force on the wall sample and the wall to lengthen. The stage was slowly extended to restore the holding force to 80 mN, followed by a fifth AFM image (Cel12A creep) of the initial area. We estimated that the applied axial forces in this experiment are similar to the value for the axial component of turgor-induced wall tension (turgor  $\times$  cross-sectional area of the 5-mm-wide strip of epidermal cell wall = 108 mN; this assumes turgor pressure of 0.6 MPa and epidermal cell depth measured as 36  $\mu\text{m}$ ; it also assumes that the axial force is largely borne by the outer epidermal wall because it is more than ten times thicker than the inner walls; tissue tensions are not included in the calculation; if they exist, they would increase forces on the outer epidermal wall).

From the two step changes in length after stress relaxation (Fig. 1c), we estimate that the reduction in force measured after the moveable stage was released (Fig. 1b) was approximately half of the actual force decay during the relaxation period. From this estimate and from the kinetics of Cel12A action (Supplementary Fig. 2), we estimated the force decay with the red broken line in Fig. 1b.

AFM imaging of the same cell wall area for the full experimental series was technically challenging because of time-dependent fouling of the AFM tip or loss of support under the imaged area. The experiment was successfully repeated three times using a total of four wall samples: The full five-image series was carried out with two samples; a third sample was used for the first three imaged points and a fourth sample was used for the last three imaged points. These data sets are shown in different colours in Fig. 1e,f.

**Image analysis.** AFM images were exported in TIFF format by Nanoscope Analysis (v 1.5). To remove shift because of sample movement during wall extension or thermal drift during AFM imaging, sets of images were aligned by the ImageJ plugin StackReg<sup>35</sup>. To calculate axial or transverse strains from the AFM images, the axial or transverse distances between five to ten pairs of stable (non-sliding) microfibril vertices were measured in ImageJ for each set of experiments. To analyse microfibril orientation, microfibrils were automatically detected by SOAX software<sup>36</sup> as ‘snakes’ (segments), which are active contours represented by a series of points that align along the intensity ridges of the image. The SOAX parameters were manually adjusted, using a snake point separation of 0.7–1 pixel. The orientation histogram was calculated by evaluating snake orientation over eight snake points for more than 28,000 snakes per image. Since long snakes contribute to the orientation histogram in proportion to their length, the contribution of short snakes in noisy parts of the image was negligible. The snakes were cut at detected snakes junctions<sup>36</sup> before evaluating their orientation, to eliminate the very small contribution of sharp angle changes at intersections. The mean snake orientations were compared at each time point by paired *t*-test from three sets of experiments. The kink angles of microfibrils were measured using the ‘Angle’ tool of ImageJ.

To identify axial shearing (side-by-side gliding) between aligned or bundled microfibrils, we looked for microfibrils with two vertices where three microfibrils intersect (Fig. 2e). When axial shearing occurs during extension, the three microfibrils should still intersect at the vertices and the distance between the two vertices should increase. Candidates for axial shearing were excluded when evidence of microfibril sliding at the vertices was seen (for example, the three microfibrils no longer intersected at a common point after extension). The microfibrils were traced on an iPad (Apple) with the ‘Forge’ software app. Colour-coded or greyscale DMT modulus images were exported with Nanoscope software (v 1.5; Bruker). To analyse the response of microfibrils and matrix separately, we used profiles of microfibril segments generated by SOAX from the Peakforce error images that were collected simultaneously with the modulus images. After blacking out four-pixel-wide snakes detected by SOAX, which correspond to the microfibrils in the modulus images, the residual modulus image represents the matrix. Subtracting the matrix image from the original modulus image gave the information for microfibrils. Histograms of the greyscale modulus images were then generated in ImageJ to analyse the stiffness responses of microfibrils and matrix to wall extension.

**Data availability.** The data that support the finding of this study are available from the corresponding author upon request.

Received 19 December 2016; accepted 22 March 2017;  
published 28 April 2017

## References

- Burton, R. A., Gidley, M. J. & Fincher, G. B. Heterogeneity in the chemistry, structure and function of plant cell walls. *Nat. Chem. Biol.* **6**, 724–732 (2010).
- Baskin, T. I. Anisotropic expansion of the plant cell wall. *Annu. Rev. Cell Dev. Biol.* **21**, 203–222 (2005).
- Cosgrove, D. J. Growth of the plant cell wall. *Nat. Rev. Mol. Cell Biol.* **6**, 850–861 (2005).
- Bidhendi, A. J. & Geitmann, A. Relating the mechanics of the primary plant cell wall to morphogenesis. *J. Exp. Bot.* **67**, 449–461 (2016).

5. Louveaux, M., Julien, J. D., Mirabet, V., Boudaoud, A. & Hamant, O. Cell division plane orientation based on tensile stress in *Arabidopsis thaliana*. *Proc. Natl Acad. Sci. USA* **113**, E4294–E4303 (2016).
6. Sampathkumar, A. *et al.* Subcellular and supracellular mechanical stress prescribes cytoskeleton behavior in *Arabidopsis* cotyledon pavement cells. *eLife* **3**, e01967 (2014).
7. Braybrook, S. A. & Jonsson, H. Shifting foundations: the mechanical cell wall and development. *Curr. Opin. Plant Biol.* **29**, 115–120 (2016).
8. Peaucelle, A. *et al.* Pectin-induced changes in cell wall mechanics underlie organ initiation in *Arabidopsis*. *Curr. Biol.* **21**, 1720–1726 (2011).
9. Kierzkowski, D. *et al.* Elastic domains regulate growth and organogenesis in the plant shoot apical meristem. *Science* **335**, 1096–1099 (2012).
10. Bassel, G. W. *et al.* Mechanical constraints imposed by 3D cellular geometry and arrangement modulate growth patterns in the *Arabidopsis* embryo. *Proc. Natl Acad. Sci. USA* **111**, 8685–8690 (2014).
11. Yanagisawa, M. *et al.* Patterning mechanisms of cytoskeletal and cell wall systems during leaf trichome morphogenesis. *Nat. Plants* **1**, 15014 (2015).
12. Nakayama, N. *et al.* Mechanical regulation of auxin-mediated growth. *Curr. Biol.* **22**, 1468–1476 (2012).
13. Preston, R. D. The case for multinet growth in growing walls of plant cells. *Planta* **155**, 356–363 (1982).
14. Suslov, D., Verbelen, J. P. & Vissenberg, K. Onion epidermis as a new model to study the control of growth anisotropy in higher plants. *J. Exp. Bot.* **60**, 4175–4187 (2009).
15. Anderson, C. T., Carroll, A., Akhmetova, L. & Somerville, C. Real-time imaging of cellulose reorientation during cell wall expansion in *Arabidopsis* roots. *Plant Physiol.* **152**, 787–796 (2010).
16. Hepworth, D. G. & Bruce, D. M. Relationships between primary plant cell wall architecture and mechanical properties for onion bulb scale epidermal cells. *J. Texture Stud.* **35**, 586–602 (2004).
17. Wilson, R. H. *et al.* The mechanical properties and molecular dynamics of plant cell wall polysaccharides studied by Fourier-transform infrared spectroscopy. *Plant Physiol.* **124**, 397–405 (2000).
18. Zhang, T., Zheng, Y. & Cosgrove, D. J. Spatial organization of cellulose microfibrils and matrix polysaccharides in primary plant cell walls as imaged by multichannel atomic force microscopy. *Plant J.* **85**, 179–192 (2016).
19. Burgert, I. & Keplinger, T. Plant micro- and nanomechanics: experimental techniques for plant cell-wall analysis. *J. Exp. Bot.* **64**, 4635–4649 (2013).
20. Park, Y. B. & Cosgrove, D. J. A revised architecture of primary cell walls based on biomechanical changes induced by substrate-specific endoglucanases. *Plant Physiol.* **158**, 1933–1943 (2012).
21. Cosgrove, D. J. Catalysts of plant cell wall loosening. *F1000Research* **5**, 119 (2016).
22. Yuan, S., Wu, Y. & Cosgrove, D. J. A fungal endoglucanase with plant cell wall extension activity. *Plant Physiol.* **127**, 324–333 (2001).
23. Schopfer, P. Biomechanics of plant growth. *Am. J. Bot.* **93**, 1415–1425 (2006).
24. Hamant, O. & Traas, J. The mechanics behind plant development. *New Phytol.* **185**, 369–385 (2010).
25. Greaves, G. N., Greer, A. L., Lakes, R. S. & Rouxel, T. Poisson's ratio and modern materials. *Nat. Mater.* **10**, 823–837 (2011).
26. Marga, F., Grandbois, M., Cosgrove, D. J. & Baskin, T. I. Cell wall extension results in the coordinate separation of parallel microfibrils: evidence from scanning electron microscopy and atomic force microscopy. *Plant J.* **43**, 181–190 (2005).
27. Fayant, P. *et al.* Finite element model of polar growth in pollen tubes. *Plant Cell* **22**, 2579–2593 (2010).
28. Park, Y. B. & Cosgrove, D. J. Xyloglucan and its interactions with other components of the growing cell wall. *Plant Cell Physiol.* **56**, 180–194 (2015).
29. Milani, P., Braybrook, S. A. & Boudaoud, A. Shrinking the hammer: micromechanical approaches to morphogenesis. *J. Exp. Bot.* **64**, 4651–4662 (2013).
30. Eichhorn, S. J. Stiff as a board: perspectives on the crystalline modulus of cellulose. *ACS Macro Lett.* **1**, 1237–1239 (2012).
31. Spatz, H., Kohler, L. & Niklas, K. J. Mechanical behaviour of plant tissues: composite materials or structures? *J. Exp. Biol.* **202**, 3269–3272 (1999).
32. Cleland, R. E. The Instron technique as a measure of immediate-past wall extensibility. *Planta* **160**, 514–520 (1984).
33. Abasolo, W. *et al.* Pectin may hinder the unfolding of xyloglucan chains during cell deformation: implications of the mechanical performance of *Arabidopsis* hypocotyls with pectin alterations. *Mol. Plant.* **2**, 990–999 (2009).
34. Cleland, R. A separation of auxin-induced cell wall loosening into its plastic and elastic components. *Physiol. Plant.* **11**, 599–609 (1958).
35. Thevenaz, P., Ruttimann, U. E. & Unser, M. A pyramid approach to subpixel registration based on intensity. *IEEE Trans. Image Process* **7**, 27–41 (1998).
36. Xu, T. *et al.* SOAX: a software for quantification of 3D biopolymer networks. *Sci. Rep.* **5**, 9081 (2015).

## Acknowledgements

This work was supported as part of the Center for LignoCellulose Structure and Formation, an Energy Frontier Research Center funded by the US Department of Energy, Office of Science, Basic Energy Sciences under award no. DE-SC0001090. D.V. was supported by NIH grant R01GM098430. We thank E. Wagner, X. Wang, S. Kiemle and Y. B. Park for technical assistance.

## Author contributions

T.Z. carried out the AFM experiments and analysed the data. D.V. assisted with SOAX analysis of microfibril orientations. D.M.D. designed and built the AFM extensometer. D.J.C. designed the research and analysed the data. T.Z., D.J.C. and D.V. wrote the manuscript.

## Additional information

**Supplementary information** is available for this paper.

**Reprints and permissions information** is available at [www.nature.com/reprints](http://www.nature.com/reprints).

**Correspondence and requests for materials** should be addressed to D.J.C.

**How to cite this article:** Zhang, T., Vavylonis, D., Durachko, D. M. & Cosgrove, D. J. Nanoscale movements of cellulose microfibrills in primary cell walls. *Nat. Plants* **3**, 17056 (2017).

**Publisher's note:** Springer Nature remains neutral with regard to jurisdictional claims in published maps and institutional affiliations.

## Competing interests

The authors declare no competing financial interests.